Molecular Switches

DOI: 10.1002/ange.201308498

An Electrochemically and Thermally Switchable Donor–Acceptor [*c*2]Daisy Chain Rotaxane**

Carson J. Bruns, Jianing Li, Marco Frasconi, Severin T. Schneebeli, Julien Iehl, Henri-Pierre Jacquot de Rouville, Samuel I. Stupp, Gregory A. Voth, and J. Fraser Stoddart**

Abstract: *Although motor proteins are essential cellular components that carry out biological processes by converting chemical energy into mechanical motion, their functions have been difficult to mimic in artificial synthetic systems. Daisy chains are a class of rotaxanes which have been targeted to serve as artificial molecular machines because their mechanically interlocked architectures enable them to contract and expand linearly, in a manner that is reminiscent of the sarcomeres of muscle tissue. The scope of external stimuli that can be used to control the musclelike motions of daisy chains remains limited, however, because of the narrow range of supramolecular motifs that have been utilized in their templated synthesis. Reported herein is a cyclic daisy chain dimer based on π-associated donor–acceptor interactions, which can be actuated with either thermal or electrochemical stimuli. Molecular dynamics simulations have shown the daisy chain's mechanism of extension/contraction in the ground state in atomistic detail.*

Molecular daisy chains[1] are a class of rotaxanes composed of self-complementary monomers with cross-threaded architectures which enable them to express extensile and contractile motions, thus earning them the title[2] of molecular muscles. Cyclic dimers, known as [*c*2]daisy chains, are of considerable interest because their large-amplitude mechanical motions can be harnessed to design artificial molecular machines[3] (AMMs) inspired by the magnificent biomolecular machines such as myosin and kinesin, which transduce chemical energy into mechanical energy to carry out the functions that sustain life processes. The actuation of switchable [*c*2]daisy chains has been controlled by ionic,[2] pH,[4] and photochemical[5] stimuli. A few pH-switchable poly[*c*2]daisy chains have also been prepared,[6] the most recent of which demonstrated[6d] a remarkable approximate 6 μm change in contour length when actuated in solution, thus bringing the dream of creating daisy chain AMMs closer to reality.[6e] Although a variety of recognition motifs have been applied to the construction of daisy chains, including transition metals,[2] crown ether cation recognition,[7] hydrophobic forces,[8] and anion binding,[9] to our knowledge, neither electrochemically switchable nor thermally switchable daisy chains have so far graced the literature. Since we and others have utilized[10] π-associated donor–acceptor (D–A) interactions to construct electrochemically switchable bistable catenanes and rotaxanes, analogous D–A daisy chains appear to us to offer new ways of controlling molecular muscles. Although there have been several reports[11] of D–A supramolecular daisy chains, that is, pseudorotaxanes, molecular daisy chains of this ilk have remained elusive. Furthermore, to our knowledge no computational analyses of [*c*2]daisy chains have been undertaken, despite their potential to deepen our understanding at the atomistic level of the structures and dynamics of mechanically interlocked architectures that exceed simple [2]rotaxanes and [2]catenanes in sophistication and complexity. Herein, we report a neutral D–A bistable [*c*2]daisy chain, based on naphthalene diimide (NDI) and a 1,5-dioxynaphthalene (DNP)-containing crown ether, along with its molecular dynamics and thermal and electrochemical switching properties in solution.

The design of the daisy chain was inspired by the NDI-based catenanes and rotaxanes introduced by the group of Sanders[12] and adapted by us[13] to construct switchable [2]rotaxanes. We decided to couple a naphtho[35]crown-10 (N35C10) macrocycle to an alkyne-terminated NDI unit so as to obtain the monomer N35C10-NDI (see the Supporting Information), which was stoppered in $CHCl_3$ with the azide-bearing stopper precursor StN_3 using a copper(I)-catalyzed azide–alkyne cycloaddition[14] (Scheme 1). Purification of the product mixture by flash column chromatography and recycling gel permeation chromatography (GPC) in $CHCl_3$ yielded the monomer **1** as the major product (68%) and the [*c*2]daisy chain **2** as the most abundant minor product (7%).

[*] C. J. Bruns, Dr. M. Frasconi, Dr. S. T. Schneebeli, Dr. J. Iehl, Dr. H.-P. Jacquot de Rouville, Prof. S. I. Stupp, Prof. J. F. Stoddart
Department of Chemistry, Northwestern University
2145 Sheridan Road, Evanston, IL 60208 (USA)
E-mail: stoddart@northwestern.edu
Dr. J. Li, Prof. G. A. Voth
Department of Chemistry, Institute for Biophysical Dynamics
James Frank Institute and Computation Institute
The University of Chicago
5735 South Ellis Avenue, Chicago, IL 60637 (USA)
E-mail: gavoth@uchicago.edu

[**] This research was supported by the Non-Equilibrium Energy Research Center (NERC), an Energy Frontiers Research Center (EFRC) funded by the US Department of Energy, Office of Science, Office of Basic Energy Sciences under Award Number DE-SC0000989. This research is part of the Joint Center of Excellence in Integrated Nano-Systems (JCIN) at King Abdulaziz City for Science and Technology (KACST) and Northwestern University (NU) (Project 34-494). The authors would like to thank both KACST and NU for their continued support of this research. J.L. and G.A.V. were supported by a grant from the Office of Naval Research (ONR Grant N00014-13-1-0058). S.T.S. thanks the International Institute for Nanotechnology (IIN) at Northwestern University (NU) for an IIN Postdoctoral Fellowship and the QUEST high-performance computing center at NU for a research allocation of computer time.

Supporting information for this article is available on the WWW under http://dx.doi.org/10.1002/anie.201308498.

 © 2014 Wiley-VCH Verlag GmbH & Co. KGaA, Weinheim

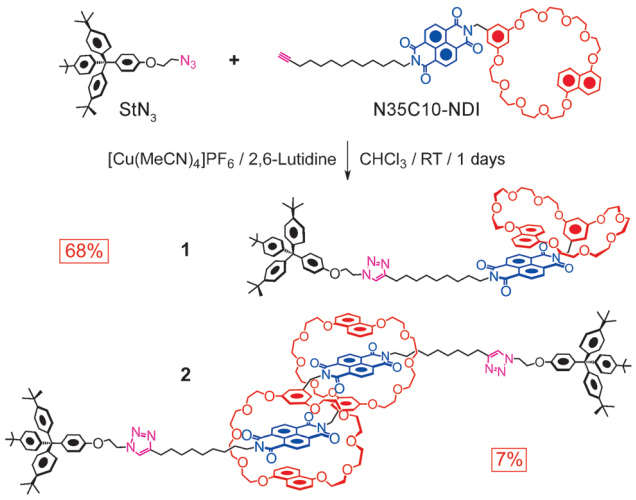

Scheme 1. Synthesis of the neutral crown ether NDI monomer **1** and the [*c*2]daisy chain **2** using the copper(I)-catalyzed azide–alkyne cycloaddition.

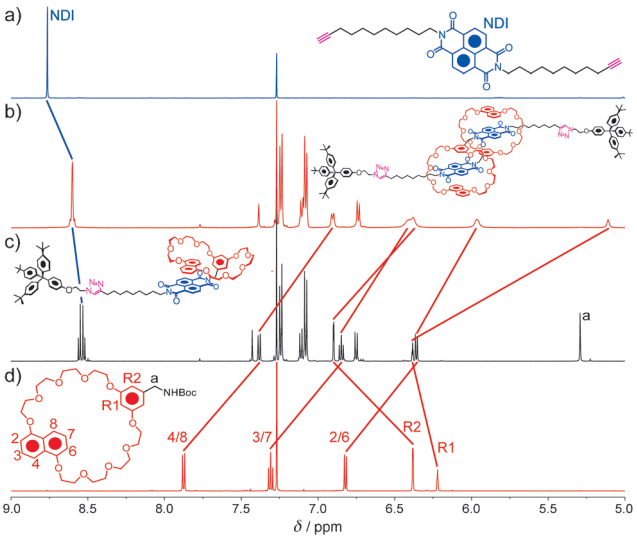

Figure 1. Partial ^{1}H NMR spectra (600 MHz, $CDCl_3$, 335 K) comparing the chemical shifts for the aromatic protons in **1** (b) and **2** (c) with those for the uncomplexed control compounds NDI($C_9H_{18}CCH)_2$ (a) and N35C10-NHBoc (d).

The compound **2** has a shorter retention time than **1** on GPC (see Figure S1a in the Supporting Information), an observation which is consistent with its larger size, while also verifying that the stopper is bulky enough to prevent the ring from deslipping over long timescales. Solutions of **1** and **2** are reddish in color, owing to a charge-transfer (CT) interaction between the NDI and DNP units in both compounds. The absorption spectra (see Figure S1b) of **1** and **2** show CT absorption bands at $\lambda_{max} = 516$ and 470 nm, respectively, with a substantially higher extinction coefficient for the CT band in the case of **2**. The existence of a stabilizing CT interaction in **1** explains the modest production of **2**, since N35C10-NDI self-complexation most likely competes with dimerization during the stoppering reaction. The high-resolution mass spectra of compounds **1** and **2** match well (see Figure S2) with the predicted spectra. Since they are composed of identical components, both compounds give rise to signals at $m/z \approx 1589$ corresponding to the $[M+H]^+$ ion of **1** and the $[M+2H]^{2+}$ ion of **2**, with isotope patterns indicative of singly and doubly charged species, respectively. We also observed the $[M+H]^+$ signal of **2** at $m/z \approx 3179$.

The ^{1}H NMR spectra of **1** and **2** were assigned (see Section S4.1) with the aid of two-dimensional ^{1}H–^{1}H correlation spectroscopy. Figure 1 presents a comparison of the chemical shifts of the aromatic protons of compounds **1** and **2** with the signals for the same protons in the uncomplexed NDI and N35C10 controls, NDI($C_9H_{18}CCH)_2$ and N35C10-NHBoc, in $CDCl_3$ at 335 K. The 2/6, 3/7, and 4/8 DNP protons as well as the NDI protons of both **1** and **2** uniformly resonate at lower frequencies compared with those of the control compounds. These shifts corroborate the evidence from the absorption spectra, thus indicating that a DNP–NDI CT interaction is being expressed in both compounds. The resonance for the crown ether's resorcinol proton H_{R1} is dramatically shifted to lower frequencies in the [*c*2]daisy chain **2** but not in the monomer **1**, an observation which is consistent with the stacking of resorcinol units on top of the NDI unit, and is expected only in the mechanically interlocked structure of the daisy chain. The significant line broadening of the NDI and crown ether signals are only observed in the case of **2**, thus indicating that the corresponding protons participate in exchange processes occurring on a timescale similar to that of the NMR timescale.

We appealed to variable-temperature (VT) ^{1}H NMR spectroscopy (Figure 2) to evaluate the dynamics of **2**. At 335 K, the exchange processes that take place in **2** are rapid enough to give a single set of time-averaged signals. These

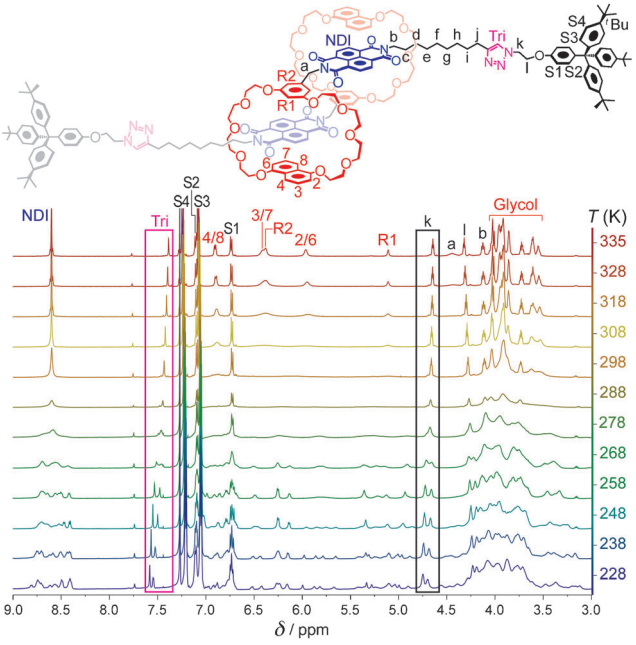

Figure 2. The VT ^{1}H NMR spectrum (600 MHz, $CDCl_3$) of **2**. The triazole proton H_{Tri} (boxed in magenta) and adjacent methylene proton H_k (boxed in black) are diagnostic signals for quantifying parameters associated with translational isomerism.

© 2014 Wiley-VCH Verlag GmbH & Co. KGaA, Weinheim

signals broaden and then separate as the temperature is lowered and exchange rates become slower on the ^{1}H NMR timescale. By contrast, the VT ^{1}H NMR spectrum (see Figure S8) of **1** shows no line broadening or coalescence over the same temperature range. The large collection of ^{1}H signals of **2** at low temperatures points to a distribution of co-conformational isomers which equilibrate slowly on the ^{1}H NMR timescale. We attribute the minor set of signals to a metastable state co-conformation (MSCC) in which the crown ether macrocycles of **2** encircle the triazole units, instead of encircling the NDI units, as expected in the ground-state co-conformation (GSCC). This conclusion is supported by the separation of the triazole proton H_{Tri} resonance and that of the adjacent methylene proton H_k, each into two sets of signals below 278 K. The more intense, higher frequency H_{Tri} signal corresponds to the GSCC, while the lower frequency signal represents the MSCC. The MSCC H_{Tri} signal undergoes a second act of separation below 248 K, most likely because the pirouetting motions of the triazole and DNP units (rotations around their central C–C bonds; see Figure S10) also enter a slow exchange regime on the ^{1}H NMR timescale. Integration of the H_{Tri} signals at 228 K reveals a GSCC/MSCC ratio of approximately 4:3. Assuming a coalescence temperature T_c of approximately 273 K for the triazole signals, the rate k_c governing the exchange between GSCC and MSCC is estimated to be 69 s^{-1}. By relying on lineshape analysis to estimate (Section S4.3) rate constants above T_c, we have calculated a free energy of activation ($\Delta G^{\neq}$) of (13.65 ± 0.04) kcal mol^{-1} for the mechanical contraction/extension motion of the bistable daisy chain. Although these parameters represent a weighted average of the activation barrier for both MSCC→GSCC and GSCC→MSCC conversions, the 4:3 GSCC/MSCC distribution corresponding to $\Delta G° < 0.2$ kcal mol^{-1} dictates that $\Delta G^{\neq}$ is nearly equal for both processes.

Computer simulation is a powerful tool, not only for validating the interpretation of experimental data, but also for elucidating the dynamics of molecular machines at the atomistic level. Although molecular dynamics (MD) simulations have played an important role in helping us to understand the one-dimensional sliding motions of rings along dumbbells in simple [2]rotaxanes,[15] little effort has been devoted to simulating and understanding the dynamics of more complex rotaxane architectures such as daisy chains. We have therefore used atomistic MD simulations in explicit $CHCl_3$ solvent to investigate the mechanism by which isomerism occurs in **2**. Since the two rings of **2** can potentially slide along their dumbbells independently of each other, two independent collective variables should be suitable to describe its correlated switching mechanism. We chose the end-to-end distance (defined as the distance between the methylene carbon atoms of the stoppers) and the ring-to-ring distance (defined as the distance between the centroids of each crown ether) as the reaction coordinates of a two-dimensional free-energy surface. At 228 K (Figure 3a), two major free-energy basins are observed, which correspond to the GSCC (Structure I) and the MSCC (Structures IV and V). The MD simulations predict the GSCC to be favored by (1.5 ± 1.2) kcal mol^{-1}, with an activation barrier to translational isomerism of approximately 12 kcal mol^{-1}, which is in reasonable agreement with the result from dynamic ^{1}H NMR spectroscopy. Remarkably, the free-energy basin corresponding to the MSCC disappears (Figure 3b) when the simulations are run at 335 K,[16] thus indicating that **2** is bistable at low temperatures and monostable at high temperatures. This unusual result most likely arises from the entropic contribution to the free energy which becomes more important at higher temperatures, since the extended state of the GSCC affords more conformational flexibility than the MSCC. The ability to control the translational isomerism of **2** with temperature provides a basis for entropy-driven[17] thermal actuation. Beyond assisting in the interpretation of experimental data, the MD calculations performed on **2** describe, in unprecedented detail, the mechanism of the GSCC→MSCC

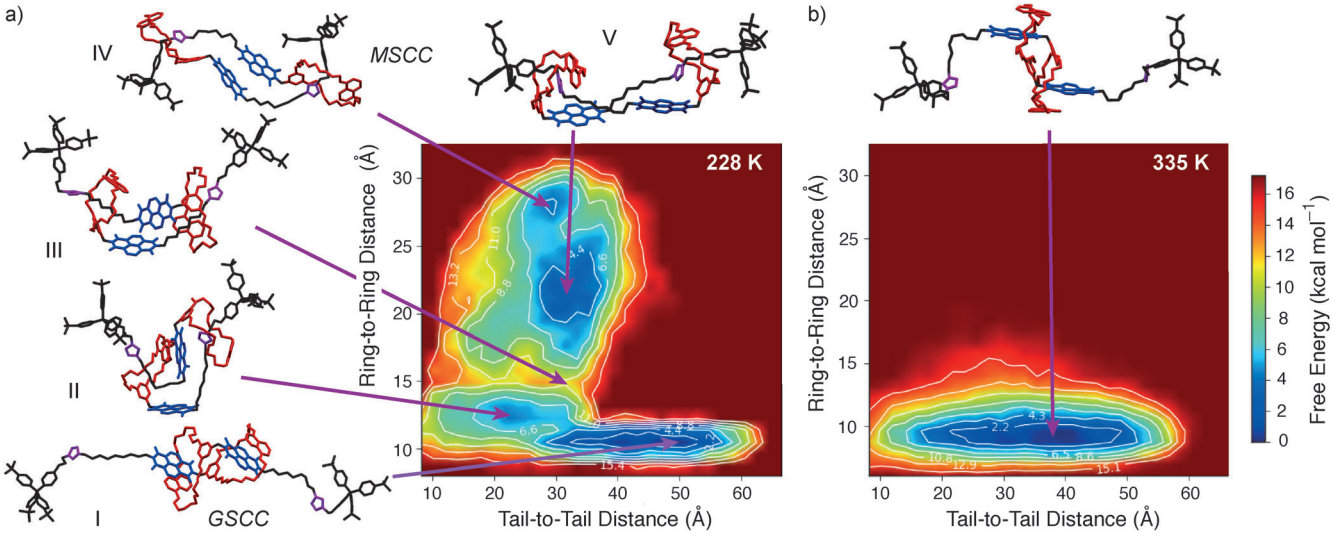

Figure 3. Two-dimensional free-energy profiles and graphical illustrations of representative structures for the translational isomerization of the [*c*2]daisy chain **2**, obtained with well-tempered metadynamics simulations in explicit $CHCl_3$ at a) 228 K and b) 335 K. These results demonstrate that temperature can be used to control the extension and contraction of **2**, since bistability is maintained only at low temperatures.

© 2014 Wiley-VCH Verlag GmbH & Co. KGaA, Weinheim

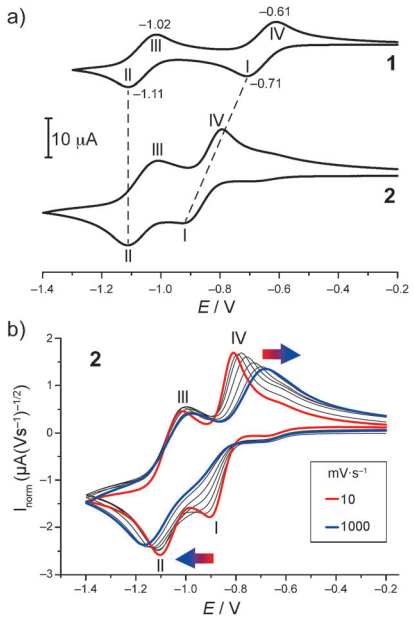

Figure 4. Cyclic voltammograms (CV) of **1** and **2** (1 mM in CH_2Cl_2, 298 K, 0.1 M NBu_4PF_6). a) A comparison between the CV of **1** and **2** at 50 $mV s^{-1}$ shows that the first reduction and final re-oxidation waves (I/IV) of **2** are dramatically shifted with respect to **1**, while the second redox couple (II/III) is identical in both compounds. b) The variable scan rate CV of **2** shows that the peak potential of processes I, II, and IV are scan-rate-dependent.

conversion. The free energy surface in Figure 3a suggests that **2** does not contract by a concerted pathway. Instead, **2** is more likely to adopt a compact, folded geometry stabilized by side-on DNP–NDI interactions (Structure II) in which only one ring encircles a triazole unit, before passing through an unstable transition state (Structure III) to access the MSCC. The MSCC, defined as any co-conformation with both rings encircling the triazole units, has a broad basin and includes a co-conformation (Structure IV) in which a side-by-side NDI–NDI interaction, reminiscent of J-aggregation, transpires. Although there is a distribution of tail-to-tail distances in both GSCC and MSCC, it is clear that the GSCC is 1–2 nm longer on average than the MSCC.

We have shown previously[13b–c] that electrochemical reduction of the NDI unit eliminates its affinity for aromatic crown-10 ethers, constituting a basis for operating a redox switch. We have used cyclic voltammetry (Figure 4) at 298 K in Ar-purged CH_2Cl_2 with 0.1 M NBu_4PF_6 as a supporting electrolyte to elucidate the redox-controlled switching mechanism of **2** at a concentration of 1 mM. All potentials are referenced against an Ag/AgCl electrode (SSCE). Since **1** is identical to the components of **2** in its constitution without being interlocked, its cyclic voltammogram (CV) is an ideal control for comparison (Figure 4a) with **2**. The CV of **1** at 50 $mV s^{-1}$ shows two reversible redox processes at $E_{1/2} = -0.66$ and -1.06 V, corresponding to the first and second reduction, respectively, of NDI. The potential of these processes are invariant (see Figure S12) over a wide range of scan rates (10–1000 $mV s^{-1}$). Each of the electron-transfer (ET) processes (I–IV in Figure 4) in the CV of **2** are discussed with respect to the two co-conformations adopted by the daisy chain, associated with the crown ethers' encirclement of either the NDI or triazole units (denoted by the prefixes "*ndi*" and "*tri*") in each of its three NDI redox states (NDI, $NDI^{\bullet-}$, and $NDI^{2(\bullet-)}$), which are populated according to the equilibrium constants K_1, K_2, and K_3, respectively (Figure 5).

(I) In **2**, process I (*ndi***2**→*ndi***2**$^{2(\bullet-)}$) is shifted to higher potentials (Figure 4a) with respect to **1** because the crown ether hinders ET to NDI. The peak broadening and increase in potential of process I at higher scan rates (Figure 4b) can be rationalized by the fact that the molecular dynamics become slow on the timescale of the CV scan, and thus a wider range of *ndi***2** (co)-conformations in which the crown ether more effectively hinders ET to NDI are sampled at the electrode. A very weak signal[18] occurring at the same potential as the control might be assignable to the MSCC (*tri***2**→*tri***2**$^{2(\bullet-)}$). This assignment is supported by a growth in intensity of the minor signal at lower temperatures (see Figure S13), since the results from ^{1}H NMR spectroscopy and MD simulations suggest that the equilibrium (K_1) shifts toward the MSCC at lower temperatures.

(II) At slow scan rates, the daisy chain has time enough to relax from *ndi***2**$^{2(\bullet-)}$ to *tri***2**$^{2(\bullet-)}$, which exposes the $NDI^{\bullet-}$ unit and yields identical potentials for process II in compounds **1** and **2**. This process is shifted to slightly higher potentials at fast scan rates, most likely because the scan rate surpasses the *ndi***2**$^{2(\bullet-)}$→*tri***2**$^{2(\bullet-)}$ conversion rate, thus leaving the $NDI^{\bullet-}$ units encircled during the generation of **2**$^{4(\bullet-)}$.

(III) The ET of process III oxidizes **2**$^{4(\bullet-)}$ back to **2**$^{2(\bullet-)}$ and is essentially identical for **1** and **2** across all scan rates.

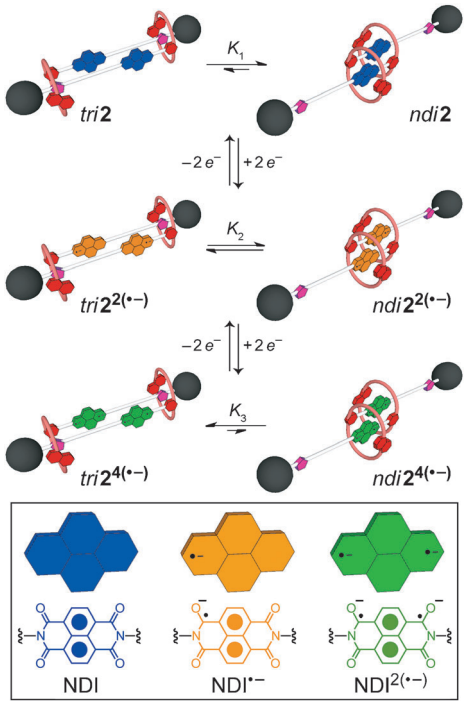

Figure 5. The electrochemical switching mechanism which governs the contractile actuation of **2**.

 © 2014 Wiley-VCH Verlag GmbH & Co. KGaA, Weinheim

Since the NDI unit is only exposed in the contracted state of the daisy chain, we conclude that *tri*$\mathbf{2}^{4(\bullet-)}$ vastly outcompetes *ndi*$\mathbf{2}^{4(\bullet-)}$ ($K_3 \ll 1$), as a shift in potential would be expected at least in the fast scan regime if *ndi*$\mathbf{2}^{4(\bullet-)}$ was populated to a significant extent.

(IV) Since the electron-rich crown ether can facilitate re-oxidation of $NDI^{\bullet-}$ by donating its electron density, the significant shift in potential of process IV in **2** with respect to **1** suggests that *ndi*$\mathbf{2}^{2(\bullet-)}$ is also well-represented in the equilibrium population. By combining this result with process II we conclude that K_2 is of intermediate strength ($K_3 < K_2 < K_1$). $\mathbf{2}^{2(\bullet-)}$ most likely equilibrates between extended and contracted states more rapidly than **2**, since having only a weak [$NDI^{\bullet-}$···crown ether] interaction will lower the activation barrier for the shuttling process.

The radical anion-driven electrochemical switching mechanism[19] portrayed in Figure 5 is further supported by spectroelectrochemical experiments, which reveal (see Figure S14) absorption bands for $\mathbf{2}^{2(\bullet-)}$ that are characteristic of NDI radical anions, with absorption maxima near $\lambda = 680$ and 750 nm.

In conclusion, we have described a neutral donor–acceptor molecular muscle having dual-mode switching capabilities controlled by stimuli, either thermal or electrochemical, which are unprecedented for molecular daisy chains. We have also demonstrated the power of molecular dynamics simulations as a means of understanding atomistically the mechanisms of isomerism occurring in daisy chains. This bistable [*c*2]daisy chain is an excellent candidate for designing artificial molecular machines that function by transducing thermal or electrochemical energy into mechanical energy on the nanoscale.

Experimental Section

Atomistic MD simulations of **2** were set up with the Desmond-Maestro package[20] using the generic OPLS-AA force field[21] in an explicit $CHCl_3$ solvent box (ca. $90 \times 90 \times 90$ Å) with periodic boundary conditions, and the constructs (ca. 30000 atoms) were equilibrated with the six-step standard protocol for 60 ps. After equilibration, well-tempered metadynamics simulations,[22] using the tail-to-tail and ring-to-ring distances as collective variables, were performed in the NPT constant ensemble (228 and 335 K, 1 bar, Martyna–Tobias–Klein coupling scheme[23]) with a 3 fs timestep. The metadynamics simulations were terminated upon convergence ($\approx$600 to 800 ns).

2: DN35C10-NDI (65 mg, 64 μmol), StN_3 (64 mg, 110 μmol), 2,6-lutidine (8 μL), and $[Cu(MeCN)_4PF_6]$ (10 mg, 27 μmol) were stirred at ambient temperature in $CHCl_3$ (700 μL) for 24 h under an atmosphere of N_2. A solution of EDTA (50 mg) in H_2O (20 mL) was added and the mixture was extracted with CH_2Cl_2 (3×10 mL). The organic extracts were combined, concentrated, and subjected to chromatography (SiO_2: eluting first with 1:3 CH_2Cl_2/EtOAc and then with 1:50 MeOH/EtOAc). The red-colored fractions were combined and further purified by recycling GPC in $CHCl_3$ to afford **1** (69 mg, 68%) and **2** (7 mg, 7%), where **2** was the faster-eluting product. ^{1}H NMR (600 MHz, $CDCl_3$, 335 K): $\delta = 8.60$ (s, 8H), 7.39 (s, 2H), 7.24 (d, $J = 8.6$ Hz, 12H), 7.10 (d, $J = 8.9$, 4H), 7.08 (d, $J = 8.6$ Hz, 12H), 6.90 (d, $J = 8.4$ Hz, 4H), 6.74 (d, $J = 8.9$ Hz, 4H), 6.41 (br, 4H), 6.38 (br, 4H), 5.96 (br, 4H), 5.11 (br, 2H), 4.64 (t, $J = 5.2$ Hz, 4H), 4.45 (br, 4H), 4.32 (t, $J = 5.2$ Hz, 4H), 4.14–4.11 (m, 4H), 4.06–4.00 (m, 12H), 3.97–3.90 (m, 28H), 3.87–3.84 (m, 8H), 3.74–3.70 (m, 4H), 3.63–3.69 (m, 8H), 3.57–3.53 (m, 4H), 2.72 (t, $J = 7.5$ Hz, 4H), 1.83 (p, $J = 7.5$ Hz, 4H), 1.71 (p, $J = 7.5$ Hz, 4H), 1.53 (p, $J = 7.5$ Hz, 4H), 1.49–1.38 (m, 16H), 1.32 ppm (s, 54H). ^{13}C NMR (150 MHz, $CDCl_3$, 335 K): $\delta = 163.3$, 162.6, 159.1, 156.0, 153.3, 152.2, 150.1, 148.6, 144.2, 141.0, 138.0, 132.5, 131.8, 131.5, 130.9, 125.6, 125.5, 125.2, 125.0, 124.1, 123.7, 121.5, 114.4, 113.4, 109.1, 103.9, 100.1, 71.5, 71.4, 71.2, 71.2, 70.2, 69.6, 67.6, 67.2, 66.8, 63.3, 53.7, 49.7, 42.6, 34.4, 31.4, 29.6, 29.5, 29.5, 29.4, 29.4, 28.4, 27.4, 25.8 ppm. HRMS (ESI-TOF-MS): *m*/*z* calcd for $C_{194}H_{227}N_{10}O_{30}$ $[M+H]^+$ 3178.6607, found 3178.6619; *m*/*z* calcd for $C_{194}H_{228}N_{10}O_{30}$ $[M+2H]^{2+}$ 1589.8340, found 1589.8376.

Received: September 30, 2013
Revised: November 3, 2013
Published online: January 21, 2014

Keywords: cyclic voltammetry · donor-acceptor systems · molecular dynamics · molecular recognition · rotaxanes

[1] J. Rotzler, M. Mayor, *Chem. Soc. Rev.* **2013**, *42*, 44–62.
[2] a) M. C. Jiménez, C. Dietrich-Buchecker, J.-P. Sauvage, *Angew. Chem.* **2000**, *112*, 3422–3425; *Angew. Chem. Int. Ed.* **2000**, *39*, 3284–3287; b) M. Jimenez-Molero, C. Dietrich-Buchecker, J.-P. Sauvage, *Chem. Eur. J.* **2002**, *8*, 1456–1466; c) M. C. Jimenez-Molero, C. Dietrich-Buchecker, J.-P. Sauvage, *Chem. Commun.* **2003**, 1613–1616; d) J.-P. Collin, C. Dietrich-Buchecker, P. Gaviña, M. C. Jimenez-Molero, J.-P. Sauvage, *Acc. Chem. Res.* **2001**, *34*, 477–487.
[3] A. Coskun, M. Banaszak, R. D. Astumian, J. F. Stoddart, B. A. Grzybowski, *Chem. Soc. Rev.* **2012**, *41*, 19–30.
[4] a) J. Wu, K. C.-F. Leung, K. D. Benítez, J.-Y. Han, S. J. Cantrill, L. Fang, J. F. Stoddart, *Angew. Chem.* **2008**, *120*, 7580–7584; *Angew. Chem. Int. Ed.* **2008**, *47*, 7470–7474; b) C. Romuald, E. Busseron, F. Coutrot, *J. Org. Chem.* **2010**, *75*, 6516–6531.
[5] R. E. Dawson, S. F. Lincoln, C. J. Easton, *Chem. Commun.* **2008**, 3980–3982.
[6] a) P. G. Clark, M. W. Day, R. H. Grubbs, *J. Am. Chem. Soc.* **2009**, *131*, 13631–13633; b) L. Fang, M. Hmadeh, J. Wu, M. A. Olson, J. M. Spruell, A. Trabolsi, Y.-W. Yang, M. Elhabiri, A.-M. Albrecht-Gary, J. F. Stoddart, *J. Am. Chem. Soc.* **2009**, *131*, 7126–7134; c) M. Hmadeh, L. Fang, A. Trabolsi, M. Elhabiri, A.-M. Albrecht-Gary, J. F. Stoddart, *J. Mater. Chem.* **2010**, *20*, 3422–3430; d) G. Du, E. Moulin, N. Jouault, E. Buhler, N. Giuseppone, *Angew. Chem.* **2012**, *124*, 12672–12676; *Angew. Chem. Int. Ed.* **2012**, *51*, 12504–12508; e) C. J. Bruns, J. F. Stoddart, *Nat. Nanotechnol.* **2012**, *8*, 9–10.
[7] a) S. J. Rowan, S. J. Cantrill, J. F. Stoddart, A. J. P. White, D. J. Williams, *Org. Lett.* **2000**, *2*, 759–762; b) S.-H. Chiu, S. J. Rowan, S. J. Cantrill, J. F. Stoddart, A. J. P. White, D. J. Williams, *Chem. Commun.* **2002**, 2948–2949; c) S. H. Ueng, S.-Y. Hsueh, C.-C. Lai, Y.-H. Liu, S.-M. Peng, S.-H. Chiu, *Chem. Commun.* **2008**, 817–819; d) E. N. Guidry, J. Li, J. F. Stoddart, R. H. Grubbs, *J. Am. Chem. Soc.* **2007**, *129*, 8944–8945; e) M. Zhang, S. Li, S. Dong, J. Chen, B. Zheng, F. Huang, *Macromolecules* **2011**, *44*, 9629–9634; f) O. A. Bozdemir, G. Barin, M. E. Belowich, A. N. Basuray, F. Beuerle, J. F. Stoddart, *Chem. Commun.* **2012**, *48*, 10401–10403.
[8] a) T. Hoshino, M. Miyauchi, Y. Kawaguchi, H. Yamaguchi, A. Harada, *J. Am. Chem. Soc.* **2000**, *122*, 9876–9877; b) L. Cao, L. Isaacs, *Org. Lett.* **2012**, *14*, 3072–3075; c) J. Rotzler, S. Drayss, O. Hampe, D. Häussinger, M. Mayor, *Chem. Eur. J.* **2013**, *19*, 2089–2101.
[9] N. H. Evans, P. D. Beer, *Chem. Eur. J.* **2011**, *17*, 10542–10546.
[10] G. Barin, A. Coskun, M. M. Foudah, J. F. Stoddart, *ChemPlusChem* **2012**, *77*, 159–185.

 © 2014 Wiley-VCH Verlag GmbH & Co. KGaA, Weinheim

[11] a) P. R. Ashton, I. W. Parsons, F. M. Raymo, J. F. Stoddart, A. J. P. White, D. J. Williams, R. Wolf, *Angew. Chem.* **1998**, *110*, 2016 – 2019; *Angew. Chem. Int. Ed.* **1998**, *37*, 1913 – 1916; b) D. Cao, C. Wang, M. A. Giesener, Z. Liu, J. F. Stoddart, *Chem. Commun.* **2012**, *48*, 6791 – 6793; c) N. Yamaguchi, D. S. Nagvekar, H. W. Gibson, *Angew. Chem.* **1998**, *110*, 2518 – 2520; *Angew. Chem. Int. Ed.* **1998**, *37*, 2361 – 2364; d) N. L. Strutt, H. Zhang, M. A. Giesener, J. Lei, J. F. Stoddart, *Chem. Commun.* **2012**, *48*, 1647 – 1649.

[12] a) D. G. Hamilton, J. K. M. Sanders, J. E. Davies, W. Clegg, S. J. Teat, *Chem. Commun.* **1997**, 897 – 898; b) D. G. Hamilton, J. E. Davies, L. Prodi, J. K. M. Sanders, *Chem. Eur. J.* **1998**, *4*, 608 – 620; c) D. G. Hamilton, M. Montalti, L. Prodi, M. Fontani, P. Zanello, J. K. M. Sanders, *Chem. Eur. J.* **2000**, *6*, 608 – 617; d) M. J. Gunter, N. Bampos, K. D. Johnstone, J. K. M. Sanders, *New J. Chem.* **2001**, *25*, 166 – 173.

[13] a) S. A. Vignon, T. Jarrosson, T. Iijima, H.-R. Tseng, J. K. M. Sanders, J. F. Stoddart, *J. Am. Chem. Soc.* **2004**, *126*, 9884 – 9885; b) T. Iijima, S. A. Vignon, H.-R. Tseng, T. Jarrosson, J. K. M. Sanders, F. Marchioni, M. Venturi, E. Apostoli, V. Balzani, J. F. Stoddart, *Chem. Eur. J.* **2004**, *10*, 6375 – 6392; c) H.-P. Jacquot de Rouville, J. Iehl, C. J. Bruns, P. L. McGrier, M. Frasconi, A. A. Sarjeant, J. F. Stoddart, *Org. Lett.* **2012**, *14*, 5188 – 5191.

[14] a) V. V. Rostovtsev, L. G. Green, V. V. Fokin, K. B. Sharpless, *Angew. Chem.* **2002**, *114*, 2708 – 2711; *Angew. Chem. Int. Ed.* **2002**, *41*, 2596 – 2599; b) C. W. Tornøe, C. Christensen, M. Meldal, *J. Org. Chem.* **2002**, *67*, 3057 – 3064.

[15] a) S. S. Jang, Y. H. Jang, Y.-H. Kim, W. A. Goddard III, A. H. Flood, B. W. Laursen, H.-R. Tseng, J.-F. Stoddart, J. O. Jeppesen, J. W. Choi, D. W. Steuerman, E. DeIonno, J. R. Heath, *J. Am. Chem. Soc.* **2005**, *127*, 1563 – 1575; b) Y. H. Jang, S. S. Jang, W. A. Goddard III, *J. Am. Chem. Soc.* **2005**, *127*, 4959 – 4964; c) S. S. Jang, Y. H. Jang, Y.-H. Kim, W. A. Goddard III, J. W. Choi, J. R. Heath, B. W. Laursen, A. H. Flood, J. F. Stoddart, K. Nørgaard, T. Bjørnholm, *J. Am. Chem. Soc.* **2005**, *127*, 14804 – 14816; d) Y. H. Jang, W. A. Goddard III, *J. Phys. Chem. B* **2006**, *110*, 7660 – 7665; e) M. E. Foster, K. Sohlberg, *J. Chem. Theory Comput.* **2007**, *3*, 2221 – 2233; f) H. Kim, W. A. Goddard III, S. S. Jang, W. R. Dichtel, J. R. Heath, J. F. Stoddart, *J. Phys. Chem. A* **2009**, *113*, 2136 – 2143; g) K. Phoa, J. B. Neaton, V. Subramanian, *Nano Lett.* **2009**, *9*, 3225 – 3229; h) Q. Zhang, Y. Tu, H. Tian, Y.-L. Zhao, J. F. Stoddart, H. Ågren, *J. Phys. Chem. B* **2010**, *114*, 6561 – 6566; i) A. Credi, M. Semeraro, S. Silvi, M. Venturi, *Antioxid. Redox Signaling* **2011**, *14*, 1119 – 1165; j) C. Casati, P. Franchi, R. Pievo, E. Mezzina, M. Lucarini, *J. Am. Chem. Soc.* **2012**, *134*, 19108 – 19117; k) A. Coskun, J. M. Spruell, G. Barin, W. R. Dichtel, A. H. Flood, Y. Y. Botros, J. F. Stoddart, *Chem. Soc. Rev.* **2012**, *41*, 4827 – 4859.

[16] To rule out any bias which may arise from incomplete sampling, MD simulations were also started from the MSCC, but these experiments always resulted in fast equilibration to the GSCC at 335 K.

[17] For a rare example of entropy-driven switching in rotaxanes, see: G. Bottari, F. Dehez, D. A. Leigh, P. J. Nash, E. M. Pérez, J. K. Y. Wong, F. Zerbetto, *Angew. Chem.* **2003**, *115*, 6066 – 6069; *Angew. Chem. Int. Ed.* **2003**, *42*, 5886 – 5889.

[18] The same sample of **2** was used for all ^{1}H NMR spectroscopic and CV experiments. Thus, the minor signal cannot be attributed to an NDI impurity because there is no evidence for such an impurity above the detection limit ($<5\%$) of ^{1}H NMR spectroscopy. A similar minor signal for process I was also observed in an analogous NDI-crown ether [2]rotaxane. See Ref. [13c].

[19] For other examples of electrochemically switchable [2]rotaxanes driven by the reduction of imide-functionalized naphthalene units, see: a) A. M. Brouwer, C. Frochot, F. G. Gatti, D. A. Leigh, L. Mottier, F. Paolucci, S. Roffia, G. W. H. Wurpel, *Science* **2001**, *291*, 2124 – 2128; b) G. Fioravanti, N. Haraszkiewicz, E. R. Kay, S. M. Mendoza, C. Bruno, M. Marcaccio, P. G. Wiering, F. Paolucci, P. Rudolf, A. M. Brouwer, D. A. Leigh, *J. Am. Chem. Soc.* **2008**, *130*, 2593 – 2601.

[20] a) Desmond Molecular Dynamics System, version 3.0, D. E. Shaw Research, New York, NY, 2011. Maestro-Desmond Interoperability Tools, version 3.0, Schrödinger, New York, NY, **2011**; b) K. J. Bowers et al., "Scalable Algorithms for Molecular Dynamics Simulations on Commodity Clusters," *Proceedings of the ACM/IEEE Conference on Supercomputing* (SC06), Tampa, Florida, **2006**, November 11 – 17; c) Z. Guo, U. Mohanty, J. Noehre, T. K. Sawyer, W. Sherman, G. Krilov, *Chem. Biol. Drug Des.* **2010**, *75*, 348 – 359; d) D. Shivakumar, J. Williams, Y. Wu, W. Damm, J. Shelley, W. Sherman, *J. Chem. Theory Comput.* **2010**, *6*, 1509 – 1519.

[21] G. A. Kaminski, R. A. Friesner, J. Tirado-Rives, W. L. Jorgensen, *J. Phys. Chem. B* **2001**, *105*, 6474 – 6487.

[22] A. Barducci, G. Bussi, M. Parrinello, *Phys. Rev. Lett.* **2008**, *100*, 020603.

[23] G. J. Martyna, D. J. Tobias, M. L. Klein, *J. Chem. Phys.* **1994**, *101*, 4177 – 4191.

 © 2014 Wiley-VCH Verlag GmbH & Co. KGaA, Weinheim